

Measures for a Multidimensional Multiverse

Hyeyoun Chung^{1,*}

¹*Center for the Fundamental Laws of Nature, Harvard University,
17 Oxford St., Cambridge, MA 02138, USA*

(Dated: August 8, 2022)

We explore the phenomenological consequences of generalizing the causal patch and scale factor cutoff measures to a multidimensional multiverse, where the vacua can have differing numbers of large dimensions. We consider a simple model in which the vacua are nucleated from a D -dimensional parent spacetime through dynamical compactification of the extra dimensions, and compute the geometric contribution to the probability distribution of observations within the multiverse for each measure. We then study how the shape of this probability distribution depends on the timescale for the existence of observers, the timescale for vacuum domination, and the timescale for curvature domination (t_{obs} , t_Λ , and t_c , respectively.) We find that in the case of the causal patch cutoff, when the bubble universes have $p + 1$ large spatial dimensions with $p \geq 2$, the shape of the probability distribution is such that we obtain the coincidence of timescales $t_{obs} \sim t_\Lambda \sim t_c$. Moreover, the size of the cosmological constant is related to the size of the landscape. However, the exact shape of the probability distribution is different in the case $p = 2$, compared to $p \geq 3$. In the case of the fat geodesic measure, the result is even more robust: the shape of the probability distribution is the same for all $p \geq 2$, and we once again obtain the coincidence $t_{obs} \sim t_\Lambda \sim t_c$. These results require only very mild conditions on the prior probability of the distribution of vacua in the landscape.

PACS numbers:

I. INTRODUCTION

The measure problem is concerned with the issue of making predictions in an eternally inflating multiverse. Eternal inflation is not a phenomenon that requires an esoteric or complicated fundamental theory in order to arise: in fact, it is a scenario that is the consequence of even the simple model of a scalar field coupled to Einstein gravity, where the potential for the scalar field is such that there is a false vacuum and a true vacuum, with a potential barrier between the two vacua. If we begin with a situation in which the scalar field assumes its false vacuum value throughout the whole of space, and if the value of the scalar field potential is positive at the false vacuum, then this provides an effective positive cosmological constant, and the spacetime undergoes eternal inflation. It is possible for the field to tunnel through the potential barrier in a region of space, thus nucleating a bubble of true vacuum in the background of false vacuum. This means that the false vacuum will never be completely eaten up by the bubbles of true vacuum, and we obtain an eternally inflating spacetime with bubbles of true vacua continuously nucleating in the background of false vacuum. As the spacetime continues growing exponentially through eternal inflation, it becomes impossible to make predictions within this multiverse by counting events, as every single event that can happen, happens infinitely many times[1].

It is thus necessary to introduce a regulator of some sort in order to define relative probabilities in the multiverse[2]. This regulator is called a *measure*. Several reasonable measures have been put forward, which give different phenomenological predictions for relative probabilities of events occurring in the multiverse[3, 6, 7, 16, 17, 19]. At first sight the existence of an eternally inflating multiverse might appear to be inconvenient and disconcerting, especially since the calculation of probabilities within such a multiverse is sensitively dependent on the choice of measure, and there is no way at present of establishing a particular choice of measure as the correct one. However, Weinberg's prediction of the cosmological constant[28] showed that the existence of a multiverse can be used to explain the smallness of the observed value of Λ , and the fact that $\Lambda \neq 0$, by using anthropic arguments. This result has become a compelling reason for studying the calculation of probabilities within a multiverse, in the hopes that we can find measures that will explain some of the observations that we make in our own universe, such as the values we measure for certain physical constants, or the coincidence of the timescales of vacuum domination, and the timescale at which observations are made[5, 8–13, 15, 18, 22, 27]. If we assume the existence of an infinite and eternally inflating multiverse, where these constants take different values in each of the bubble universes, then it could be that we are highly

*Electronic address: hyeyoun@physics.harvard.edu.

likely to find ourselves in a universe where the parameters of physical theories take the values that we observe.

The list of measures that have been proposed so far can be divided into two broad categories: *global* measures, and *local* measures[2]. Global measures define a notion of a time t on the entire spacetime, and calculate the probability of an event A by counting the number of times A occurs before a cutoff time $t = t_0$. Local measures construct an ensemble of geodesics in the spacetime, count the number of times A occurs in a neighborhood of each geodesic, and then take the ensemble average (the specification of initial conditions for the geodesics is part of the definition of a local measure.) There is no consensus on which of the existing measure proposals is correct: however, it is possible to rule out some measures by insisting that the predictions made by the measures should be consistent with our observations of our own universe. For example, the proper time measure[14] has been discredited, as it predicts that our universe should be much younger than it is, with double-exponential probability.

One limitation of the existing measure proposals, and the analysis of their properties, is that almost all of the work done to date has assumed that all of the vacua in the multiverse are $(3 + 1)$ -dimensional; however, there is no guarantee that this is the case. In fact, it is easy to envision a fundamental theory which allows for the nucleation of vacua with different numbers of large dimensions, with the extra dimensions being compactified on an internal manifold: the string theory landscape, for example, is expected to contain a large landscape of vacua with different numbers of dimensions.

This point naturally raises two questions: firstly, can the existing measure proposals be generalized to the case of a multi-dimensional multiverse? And secondly, are these generalizations robust? That is, are any major qualitative differences in the phenomenological predictions of these measures as compared to the case in which all the vacua are $(3+1)$ -dimensional? Nomura has recently proposed a measure[24, 25] that he points out is fully applicable in its present form to the case of arbitrary numbers of large and compact dimensions (although it is also possible to apply the measure to the case of $3+1$ -dimensions by integrating out the other dimensions.) Blanco-Pillado and Vilenkin have generalized the well-known scale factor measure to the case of a multi-dimensional multiverse[23], and have shown that the generalization avoids the Youngness Paradox to the same degree as the original scale factor measure.

There is still much work to be done in investigating the phenomenological aspects of multi-dimensional measures, however, and we address that problem in this paper. First we consider two local measures that have been found to be phenomenologically satisfactory in the case of $(3+1)$ -dimensional vacua—the causal patch measure[16, 17], and the fat geodesic measure[2, 6, 7]—and generalize them straightforwardly to the case of a multi-dimensional multiverse. We then study how these measures can be used to predict the timescales of vacuum domination, curvature domination, and observation (t_Λ , t_c , and t_{obs}) in the various vacua, by applying the measures to a specific, yet sufficiently generic model of a multiverse with vacua of differing numbers of large dimensions.

In this work we follow the approach of Bouusso et al., who investigated the ways in which the geometry of various measures could affect their phenomenological predictions[22, 27]. The general method is to determine the probability distribution of observations in the multiverse over the three timescales t_Λ , t_c , and t_{obs} , by factoring the distribution into a part corresponding to the prior probability of the formation of bubbles characterized by the parameters (t_Λ, t_c) , a part corresponding to the density of observers per unit mass per logarithmic time interval, averaged over the different types of bubbles, and a part corresponding to the mass inside the cutoff. By arguing that the first two factors have a constrained form that we can determine through logical reasoning, and that the leading contribution to the probability distribution comes from the third and last term, which can be explicitly calculated, we can then study important features of the probability distribution.

There are several ways in which the probability distribution of observations calculated in this manner could display some qualitative differences in the multi-dimensional case, as compared to the $(3+1)$ -dimensional case. If we assume that the vacuum bubbles in the multi-dimensional case are open FRW universes with the extra dimensions compactified on a sphere, then the evolution of the FRW scale factor inside the bubble, and thus the mass contained inside the cutoff, will depend on the number of large dimensions. The parameter t_Λ , which is related to the effective cosmological constant inside the bubble, is also related to the number of large dimensions. Thus the probability distribution could change depending on the number of large dimensions there are in the bubbles that we are considering. Moreover, the probability distribution could depend, not just on the number of large dimensions in the bubble, but the number of large dimensions relative to the total dimension D of the original higher-dimensional space. In practice we find that the shape of the probability distribution is largely determined by just one factor: the number of large dimensions in the bubble. For the causal patch measure, the results can be classed into three main groups: the case of 2 large spatial dimensions, 3 large spatial dimensions, and all spatial dimensions larger than three. However, although the probability distributions differ in all three cases, for 3 spatial dimensions or larger, we predict the coincidence $t_{obs} \sim t_\Lambda \sim t_c$. For the fat geodesic measure, the results can be classed into two groups: the case of 2 large spatial dimensions, and the case of 3 or more large spatial dimensions. Finally, for both the causal patch measure and the fat geodesic measure, the smallness of the cosmological constant is related to the number of vacua in the multiverse.

This paper is structured as follows. In Section II, we describe the causal patch and fat geodesic measures and outline how they can be generalized to the case of a multiverse with multi-dimensional vacua. In Section IV, we

describe the specific model that we will use for such a multiverse, so that we can carry out concrete calculations using the measures. In Section VI we explore the phenomenological properties of the measures by applying them to this multiverse model. We conclude in Section VII.

II. THE MEASURES AND THEIR GENERALIZATIONS TO A MULTI-DIMENSIONAL MULTIVERSE

We can immediately generalize two well-known measures to the case of a multi-dimensional multiverse: the *causal patch* measure, and the *fat geodesic* measure. Both are local measures, which define the relative probabilities of different events by only counting events in a finite neighborhood of a single inextendible timelike geodesic in the multiverse (where the neighborhood is defined differently for each measure), and then taking an average over initial conditions and possible decoherent histories for the geodesic. If N_I is the number of times that outcome I occurs within the specified neighborhood of the geodesic, and $\langle N_I \rangle$ indicates the expectation value after averaging over initial conditions and decoherent histories, then the relative probability of outcomes I and J are given by:

$$\frac{p_I}{p_J} = \frac{\langle N_I \rangle}{\langle N_J \rangle} \quad (1)$$

We can find the expectation value $\langle N_I \rangle$ by constructing an ensemble of geodesics, and then taking the ensemble average. This is done by selecting an initial spacelike hypersurface Σ_0 , and then constructing a geodesic orthogonal to that hypersurface. If we then take Z identical copies of Σ_0 and choose the same starting point for the geodesic in each copy, the resulting Z geodesics, and their corresponding neighborhoods, represent different decoherent histories for the multiverse. In order to account for different initial conditions, we can then take a weighted average over different initial surfaces Σ_0 , which correspond to different initial vacua.

The **causal patch measure** is a local measure for which the local neighborhood of the geodesic is taken to be the causal patch of the endpoint of the geodesic. The **fat geodesic measure** is a local measure for which the local neighborhood of the geodesic is a fixed infinitesimal orthogonal cross-sectional volume dV , which we take to be spherical. Both of these measures can be directly generalized to the case of a multidimensional multiverse with no change in their definitions.

III. DETERMINING THE PROBABILITY DISTRIBUTION OF OBSERVATIONS

In this section we outline the general approach taken in [22, 27] to determine the essential features of the probability distribution of observations in the multiverse. Every observation can be labelled within the cutoff region determined by the measure, with the three parameters $(\log t_{obs}, \log t_c, \log t_\Lambda)$. We would like to obtain as much information as possible about the probability distribution of observations over these parameters. We first define the *prior probability distribution*

$$\frac{d^2 \tilde{p}}{d \log t_\Lambda d \log t_c}, \quad (2)$$

which is the probability density to nucleate a bubble with the given values of the parameters $\log t_c, \log t_\Lambda$ inside the cutoff region.

We then assume that the probability density for observations within a given bubble of vacuum i has the form

$$\frac{dN_i}{d \log t_{obs}} \sim M(\log t_{obs}, \log t_c, \log t_\Lambda) \times \alpha_i(\log t_{obs}, \log t_c, \log t_\Lambda), \quad (3)$$

where M is the mass inside the cutoff region, and α_i is the number of observations per unit mass per logarithmic time interval inside a bubble of type i . This decomposition separates the information about the cutoff procedure (contained in M) from information about the particular vacuum i (which is contained in α_i .) We now average α_i over the bubbles with a given $(\log t_\Lambda, \log t_c)$, to get the average number of observations per unit mass per logarithmic time, α . Thus the full probability distribution over all three variables is

$$\frac{d^3 p}{d \log t_{obs} d \log t_\Lambda d \log t_c} = \frac{d^2 \tilde{p}}{d \log t_\Lambda d \log t_c} \times M(\log t_{obs}, \log t_c, \log t_\Lambda) \times \alpha(\log t_{obs}, \log t_c, \log t_\Lambda). \quad (4)$$

It is possible to calculate M explicitly for each cutoff, as it is a purely geometrical factor. We carry out this calculation in Section VI, for both the causal patch and fat geodesic cutoffs. We also argue that α can be written as a function

purely of $\log t_{obs}$, which requires only weak assumptions. Furthermore, we expand the form of the prior probability density \tilde{p} as:

$$\frac{d^2 \tilde{p}}{d \log t_\Lambda d \log t_c} \sim t_\Lambda^{-2} g(\log t_c) \quad (5)$$

for some function $g(\log t_c)$, as we are considering small values of $\Lambda \sim t_\Lambda^{-2}$ and can thus Taylor expand in Λ .

IV. A MODEL FOR A MULTI-DIMENSIONAL MULTIVERSE

In order to explicitly explore the phenomenological predictions of these generalized measures, we must specify a concrete model for a multiverse where the vacua can have different numbers of large dimensions, and apply the measures to this model. We would like the model to be fairly generic, so that we can identify the qualitative properties of the measures that result from extending them to multi-dimensional models, without our results being too much influenced by the particular model we have chosen.

Starting with a fundamental theory in D -dimensions, we would like to consider a model that allows for the dynamic nucleation of vacua with varying numbers of large dimensions, while the remaining spatial dimensions are compactified. In general, the Lagrangian for the fundamental theory will have the form

$$S = \int d^D X \sqrt{-G} \left[M_D^{D-2} \mathcal{R} + \mathcal{L}(\psi) + \hat{\mathcal{L}}(\mathcal{R}) \right], \quad (6)$$

where X are the coordinates on the full D -dimensional spacetime, G is the metric on the spacetime, M_D is the D -dimensional Planck mass, \mathcal{R} is the Ricci scalar, and $\mathcal{L}(\psi)$ is the lagrangian representing the contribution of generic matter sources. The term $\hat{\mathcal{L}}(\mathcal{R})$ represents possible corrections to the Einstein-Hilbert Lagrangian that involve higher powers of curvature. In this work we assume that there are no terms that mix ψ and \mathcal{R} .

Theories of this form were studied by Giddings in [21], where the metric was assumed to have the form

$$ds^2 = e^{2A(y)} ds_4^2 + R^2(x) g_{mn}(y) dy^m dy^n, \quad (7)$$

where ds_4^2 is the metric for (3+1)-dimensional de Sitter space. There are four large dimensions, and $D - 4$ compact dimensions. A radial dilaton field $R(x) = e^{\phi(x)}$, that depends only on the coordinates of the large dimensions, encodes the size of the compact dimensions. By assuming that $R(x)$ varies slowly on scales of order the compactification size, the equations for the matter fields can be solved to give $\psi = \psi_0$. Substituting these solutions into the full action, and then integrating over the compact dimensions, gives an effective potential for the radial dilaton. The dimensionally reduced action has the form:

$$S = \int d^4 x \sqrt{-g_4} \left[\mathcal{R}_4 - \frac{1}{2} (D-4)(D-2) (\nabla \phi)^2 + V(\phi) \right] \quad (8)$$

where $V(\phi)$ is the effective potential for $\phi(x)$. Thus the dimensionally reduced theory has the form of Einstein gravity in (3+1) dimensions coupled to a scalar field, the radial dilaton, whose dynamics are governed by an effective potential $V(\phi)$.

If this potential has stable or metastable local minima, then the nucleation of vacua with different numbers of large dimensions is possible in this theory. For example, if the potential has a local minimum such that the value of the potential at that minimum is positive, then this corresponds to a positive cosmological constant in the dimensionally reduced theory. The local minimum is a stable solution for the dilaton field, and so represents a de Sitter vacuum in (3 + 1) dimensions where the extra dimensions are compactified on a $D - 4$ -dimensional sphere. If the value of the potential at the local minimum is negative, then the minimum is an AdS vacuum in (3 + 1) dimensions; if the value of the potential is zero, then the minimum is a Minkowski vacuum. It is also possible for the effective potential to have several local minima and thus allow for several possible vacua. It is possible that some or all of these vacua are metastable; however, if the decay rates of these vacua are sufficiently low, then the metastable vacua correspond to valid, viable universes within the multiverse that could exist for long enough for observers to evolve.

The nucleation of a (3 + 1)-dimensional vacuum in this theory can occur through the process of *compactification*, which is exactly analogous to the nucleation of bubbles via Coleman-DeLuccia or Hawking-Moss instantons. In the Coleman-DeLuccia instanton, we consider a scalar field coupled to Einstein gravity that is in its false vacuum state throughout the whole of space. This corresponds to the scalar field taking its value at a local minimum of its potential. A vacuum of true vacuum can nucleate within the false vacuum, if the scalar field tunnels through the potential barrier

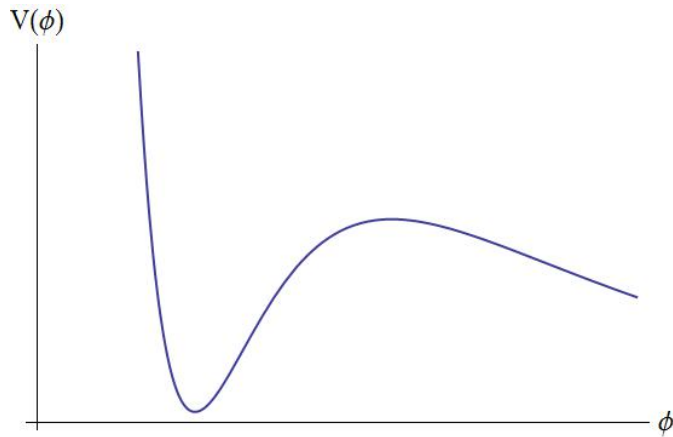


FIG. 1: An effective potential for the radial dilaton field $\phi(x)$ that has a metastable minimum corresponding to a vacuum with a positive effective cosmological constant.

to the global minimum of the potential. In the Hawking-Moss instanton, a bubble is nucleated in which the scalar field has tunneled to its value at a local *maximum* of the potential, and then rolls down into the global minimum, so that the bubble becomes a bubble of true vacuum. If we think of the radion field $\phi(x)$ as a scalar field coupled to gravity in the $(3 + 1)$ large dimensions, then bubbles of vacua can nucleate in which $\phi(x)$ takes its values at local minima of the potential, which corresponds to the extra dimensions being compactified.

Giddings considers various possible matter sources for the dilaton potential, including fluxes in the compact dimensions, and branes wrapped around the compact dimensions. In both cases, he finds that the sources contribute terms to the effective potential that are exponentials of the dilaton field $\phi(x)$. Thus we can generically assume that the effective potential for $\phi(x)$ is a sum of exponentials of $\phi(x)$.

One explicit model of this form is that discussed by Carroll, Johnson, and Randall in [26], which considers a fundamental theory of Einstein gravity in D dimensions with a cosmological constant, coupled to one or more q -form field strengths. The action for the higher-dimensional theory is:

$$S_D = \frac{1}{2} \int d^D x \sqrt{-\tilde{g}^{(D)}} \left(\tilde{\mathcal{R}}^{(D)} - 2\Lambda_D - \frac{1}{2q!} \tilde{F}_q^2 \right), \quad (9)$$

where we have used Λ_D to denote the D -dimensional cosmological constant in order to distinguish it from the effective cosmological constant inside the FRW bubble universes that we will describe later. Assuming spherical symmetry in the compact dimensions, we can write the metric in the form

$$ds^2 = \tilde{g}_{\mu\nu}^{p+2}(\mathbf{x}) dx^\mu dx^\nu + R^2(\mathbf{x}) d\Omega_q^2, \quad (10)$$

where we have decomposed the metric into $(p + 2)$ large dimensions and q compact dimensions, and the entire space has $D = p + 2 + q$ dimensions. The radion field $R(x)$ and the $p + 2$ -dimensional metric $\tilde{g}_{\mu\nu}^{p+2}$ are functions of the $p + 2$ -dimensional coordinates x . The magnetic q -form field strengths solving Maxwell's equations and respecting the q -dimensional spherical symmetry are given by

$$\tilde{F}_q = Q \sin^{q-1} \theta_1 \dots \sin \theta_{q-1} d\theta_1 \wedge \dots \wedge d\theta_q \quad (11)$$

We consider solutions with only a single fixed q , so that multiple q -form charges are not turned on simultaneously. We can now integrate over the q compact dimensions to obtain the dimensionally reduced theory in $p + 2$ dimensions. We also perform a conformal transformation in order to express our results in the $p + 2$ -dimensional Einstein frame, so that we can view the theory as Einstein gravity coupled to a scalar field. The conformal transformation is

$$g_{\mu\nu} = R^{\frac{2q}{p}} \tilde{g}_{\mu\nu} \quad (12)$$

and the dimensionally reduced action in the Einstein frame is

$$S_{p+2} = \int d^{p+2} x \sqrt{-g} \left[\frac{1}{2} \mathcal{R} - \frac{1}{2} \frac{q(p+q)}{pR^2} g^{\mu\nu} \partial_\mu R \partial_\nu R - V(R) \right], \quad (13)$$

where $V(R)$ is an effective potential for the radion field $R(x)$. We can define a canonically normalized radion field ϕ by making the change of variables

$$R = \exp \left[\sqrt{\frac{p}{q(p+q)}} \frac{\phi}{M_{p+2}} \right] \quad (14)$$

In terms of ϕ , the dimensionally reduced action is

$$S_{p+2} = \int d^{p+2}x \sqrt{-g} \left[\frac{1}{2} \mathcal{R} - \frac{1}{2} g^{\mu\nu} \partial_\mu \phi \partial_\nu \phi - V(\phi) \right] \quad (15)$$

where the effective potential $V(\phi)$ is

$$V(\phi) = \frac{1}{2} \left[-q(q-1) \exp \left(-2\sqrt{\frac{p+q}{pq}} \phi \right) + 2\Lambda_D \exp \left(-2\sqrt{\frac{q}{p(p+q)}} \phi \right) + \frac{Q^2}{2} \exp \left(-2(p+1)\sqrt{\frac{q}{p(p+q)}} \phi \right) \right] \quad (16)$$

In general, we can have J copies of a q -form, with e_i being the gauge coupling for each copy, and n_i being the number of units of fundamental charge, in which case Q in the above formula is replaced with

$$Q^2 \equiv \sum_{i=1}^J Q_i^2 = \sum_{i=1}^J e_i^2 n_i^2. \quad (17)$$

Thus, for a given number D of dimensions in the fundamental theory, we have three independent parameters that we can vary: the number of compact dimensions q , the charge Q , and the higher-dimensional cosmological constant Λ_D . These parameters determine the form of the effective potential $V(\phi)$.

The possible forms $V(\phi)$ were studied in [26], and it was found that we require $\Lambda_D \neq 0$ for the existence of solutions that allow for the dynamical nucleation of bubbles with compactified dimensions. The results are qualitatively similar when $\Lambda_D < 0$ compared to when $\Lambda_D > 0$, so we will only consider the case $\Lambda_D > 0$. For certain values of Q , the effective potential can have a local minimum and a local maximum, showing that there can be $p+2$ -dimensional metastable vacua. The value of the potential at the local minimum can be positive, zero, or negative, so that the metastable vacua can be de Sitter, Minkowski, or Anti de Sitter.

We would like to further generalize this model to allow for the presence of pressureless macroscopic matter, so that we can have regions of matter, curvature, and vacuum domination inside the bubbles nucleated in the multiverse. This can be done quite easily by using the Einstein equations in the $p+2$ -dimensional Einstein frame:

$$R_{\mu\nu} - \frac{1}{2} g_{\mu\nu} R = T_{\mu\nu}, \quad (18)$$

where we have chosen units so that $8\pi G = 1$. If we compute the Ricci tensor and Ricci scalar for the $p+2$ -dimensional metric $g_{\mu\nu}$, then on the right-hand side we can substitute the energy-momentum tensor $T_{\mu\nu}$ by summing the energy-momentum tensor for the scalar field ϕ , and the energy-momentum tensor for pressureless matter, which has the form

$$T_{\text{matter}}^{\mu\nu} = \rho U^\mu U^\nu \quad \text{for} \quad \mu = \nu = 0 \quad (19)$$

$$T_{\text{matter}}^{\mu\nu} = 0 \quad \text{otherwise.}, \quad (20)$$

for some constant density ρ , where the density is calculated with respect to the large dimensions (as we are considering macroscopic matter.)

V. OPEN FRW UNIVERSES WITH COMPACTIFIED DIMENSIONS

In order to compute the mass contained within the cutoff region, the calculation in [22, 27] proceeds by assuming that every bubble in the multiverse is an open FRW universe, as is usually formed by Coleman-deLuccia tunneling. The metric has the form:

$$ds^2 = -dt^2 + a(t)^2 (d\chi^2 + \sinh^2 \chi d\Omega^2) \quad (21)$$

The Friedmann equations for $a(t)$ have the form

$$\left(\frac{\dot{a}}{a} \right)^2 = \frac{t_c}{a^3} + \frac{1}{a^2} \pm \frac{1}{t_\Lambda^2} \quad (22)$$

and can be solved for $a(t)$ piecewise, in terms of t_Λ, t_c , by ignoring all but one term on the right-hand side for each region in time. The nature of the solution depends on whether the cosmological constant Λ (related to $t_\Lambda = \sqrt{3/|\Lambda|}$) is positive or negative, and whether $t_c \gg t_\Lambda$ or $t_c \ll t_\Lambda$.

We can adapt this analysis to our model (though in this work we will only consider positive cosmological constant $\Lambda > 0$.) A bubble universe can nucleate in the background D -dimensional multiverse through a process analogous to Coleman-DeLuccia tunneling[26], with the radion field ϕ playing the role of the scalar field in the CdL instanton, as described in Section IV. The spacetime after nucleation is given by a configuration analogous to a thick-walled CdL bubble. The region inside the bubble is given by an open FRW universe, where the metric in the $p + 2$ -dimensional Einstein frame has the form

$$ds^2 = -dt^2 + a(t)^2(d\chi^2 + \sinh^2 \chi d\Omega_p^2) \quad (23)$$

In order to match to the solution outside the bubble, the solution inside the bubble must satisfy the conditions $a = 0, \dot{\phi} = 0$ at $t = 0$.

The equations of motion for $a(t)$ and $\phi(t)$ give us the multi-dimensional analogue of Friedmann equations, which take the form:

$$\left(\frac{\dot{a}}{a}\right)^2 = \frac{t_c^{p-1}}{a^{p+1}} + \frac{1}{a^2} \pm \frac{1}{t_\Lambda^2} + \frac{2}{p(p+1)} \left(\frac{\dot{\phi}^2}{2} + V(\phi) - V_0\right) \quad (24)$$

$$\ddot{\phi} + (p+1)\frac{\dot{a}}{a}\dot{\phi} = -V'(\phi) \quad (25)$$

where $V(\phi)$ is the potential for ϕ , and V_0 is the constant part of $V(\phi)$ (which gives the cosmological constant term $\frac{1}{t_\Lambda^2}$.) The term $\frac{t_c^{p-1}}{a^{p+1}}$ on the righthand side of the Friedmann equation for $a(t)$ corresponds to the contribution of non-dynamical, pressureless matter. We assume that the matter is macroscopic, so that it scales as $\sim \frac{1}{a^{p+1}}$. It would also be possible to analyze the effect of microscopic matter that is at the scale of the compact dimensions, by introducing a term $\sim \frac{1}{a^{p+1}R^q}$, where R is the radion field. Preliminary computations indicates that this does not make a significant qualitative difference to our results, so we will consider only macroscopic matter in this paper and leave a more detailed analysis to a future work.

We cannot solve these equations analytically. However, we can solve them numerically. The potential $V(\phi)$ can be specified following the model given in [26] (which, as shown in [21], is a fairly generic potential that can be obtained by dimensionally reducing different fundamental theories.) The potential depends on the number of large spatial dimensions $(p + 1)$, the number of compact dimensions q , the cosmological constant in the full $p + 2 + q$ -dimensional theory Λ , and the sum of charges of the q -form fluxes in the compact dimensions, Q . By scanning over these parameters, we can find a large set of solutions for different values of t_c and t_Λ , and see how these solutions vary with each of the parameters.

In general, a solution for a bubble is obtained through a Coleman-DeLuccia instanton for ϕ , where ϕ tunnels through a potential barrier in $V(\phi)$ before emerging at some value ϕ_- , and then rolls down into a local minimum of $V(\phi)$, then oscillates about that minimum before settling down to a constant value, to give an FRW universe with q compact dimensions with ϕ at some finite value ϕ_{min} . If the value of the potential at ϕ_{min} is positive then we obtain an asymptotically de Sitter bubble, and $a(t)$ increases monotonically from zero to infinity, and if the value of the potential at ϕ_{min} is positive then we obtain an asymptotically AdS bubble, and $a(t)$ crunches back to zero. If the value of the potential at ϕ_{min} is zero, then we obtain an asymptotically M_{p+2} bubble.

Thus, technically we would need to calculate the value ϕ_- in order to obtain the correct initial value of ϕ within the FRW bubble. However, we have verified numerically that starting with a fairly arbitrary initial value of ϕ_- , between the local minimum and local maximum of the potential, does not significantly affect the final solutions $a(t), \phi(t)$. Therefore, as it is difficult to compute the CdL instanton precisely, in order to numerically solve the Friedmann equations we start with an arbitrary initial value for $\phi(t)$, chosen to be halfway between the values of ϕ at the local minimum and local maximum of the effective potential.

VI. THE PHENOMENOLOGY OF THE MEASURES

We can now proceed to calculate the mass contained within the cutoff in a typical bubble, and thus find part of the contribution to the probability distribution of observations in the multiverse.

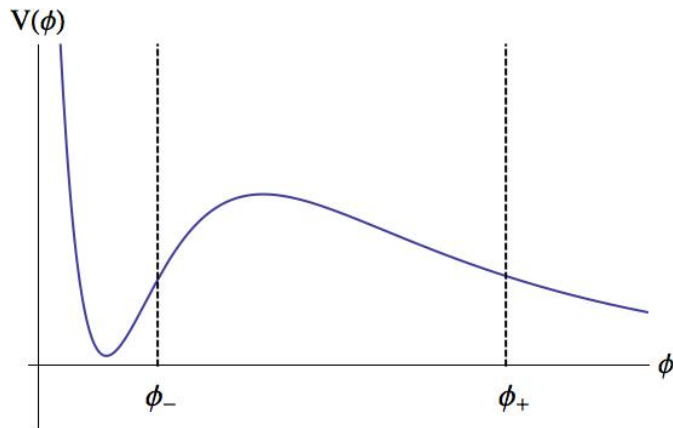


FIG. 2: An effective potential for the radial dilaton field $\phi(x)$ that has a metastable minimum corresponding to a vacuum with a positive effective cosmological constant. Compactification can occur dynamically when the field ϕ tunnels through the potential barrier between ϕ_+ and ϕ_- , and then rolls down into a local minimum of $V(\phi)$, which corresponds to a de Sitter universe in this case, as the value of $V(\phi)$ at this minimum is positive.

A. The causal patch measure

For the causal patch measure, we may place the origin of the bubble of interest at the center of the causal patch, by boost symmetry. The boundary of the causal patch is given by the past light-cone from the future end point of the comoving geodesic at the origin, $\chi = 0$:

$$\chi_{CP}(t) = \int_t^{t_f} \frac{1}{a(t')} dt' \quad (26)$$

As we are only considering $\Lambda > 0$, where Λ is the effective cosmological constant inside the bubble (as opposed to the D -dimensional cosmological constant Λ_D), then the causal patch coincides with the event horizon, and may be computed as if the de Sitter vacuum were eternal ($t_f \rightarrow \infty$), as the correction from late-time decay is negligible.

The volume available to observers at t_{obs} may be calculated by:

$$V_{CP} = \mathcal{S}[\chi_{CP}(t_{obs})], \quad (27)$$

where $\mathcal{S}[\chi]$ is the comoving volume inside a sphere of radius χ . The mass inside this volume is then given by $M_{CP} = \rho a^{p+1} V_{CP} = t_c^{p-1} V_{CP}$. The probability distribution of observations made in the landscape is then given by:

$$\frac{d^3 p}{d \log t_{obs} d \log t_{\Lambda} d \log t_c} \sim t_{\Lambda}^{-2} g(\log t_c) \times \alpha(\log t_{obs}, \log t_c, \log t_{\Lambda}) \times M_{CP}(\log t_{obs}, \log t_c, \log t_{\Lambda}) \quad (28)$$

If we assume that the factors $g(\log t_{obs})$ and $\alpha(\log t_{obs}, \log t_{\Lambda}, \log t_c)$ do not provide the leading contributions to the probability distribution, but rather the factor $M(\log t_{obs}, \log t_{\Lambda}, \log t_c)$ does, then we can calculate the contribution of M_{CP} to the probability density and analyze the resulting trends.

In order to calculate the probability distribution over the three variables $t_{obs}, t_{\Lambda}, t_c$, we considered a range of p and q , and identified values of the parameters Q and Λ that would give a potential with a positive-valued local minimum, so that we could look at vacua with a positive effective cosmological constant. Scanning over different ranges of Q and Λ gave us a range of t_{Λ} to work with. We solved the differential equations for $a(t)$ and $\phi(t)$ for a large range of t_{Λ} and t_c (where t_c was input by hand), and then calculated M_{CP} for a range of t_{obs} , choosing values for the three time scales so that they were well separated. We considered the following regions of parameter space:

$$\text{Region I} \quad t_{obs} < t_c < t_{\Lambda} \quad (29)$$

$$\text{Region II} \quad t_c < t_{obs} < t_{\Lambda} \quad (30)$$

$$\text{Region III} \quad t_c < t_{\Lambda} < t_{obs} \quad (31)$$

$$\text{Region IV} \quad t_{\Lambda} < t_{obs} \quad (32)$$

$$\text{Region V} \quad t_{obs} < t_{\Lambda} \quad (33)$$

$$(34)$$

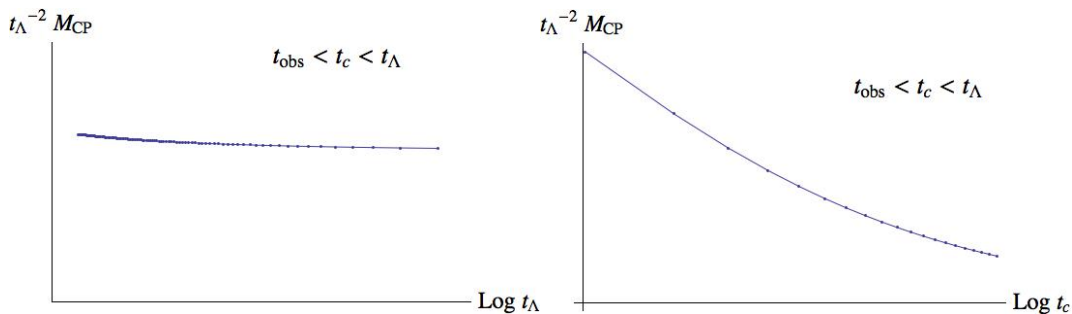


FIG. 3: Typical probability distributions obtained using the causal patch cutoff over $\log t_\Lambda$ for fixed $\log t_c$, and $\log t_c$ for fixed $\log t_\Lambda$, in the case $p = 2$, in Region I of parameter space, corresponding to $t_{obs} < t_c < t_\Lambda$. The specific parameters used here are ($p = 2, q = 2, Q = 3.2, \Lambda = 0.1$).

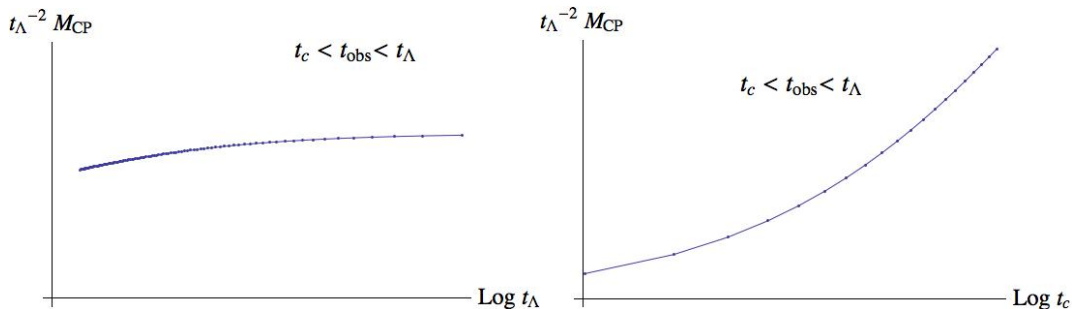


FIG. 4: Typical probability distributions obtained using the causal patch cutoff over $\log t_\Lambda$ for fixed $\log t_c$, and $\log t_c$ for fixed $\log t_\Lambda$, in the case $p = 2$, in Region II of parameter space, corresponding to $t_c < t_{obs} < t_\Lambda$. The specific parameters used here are ($p = 2, q = 2, Q = 3.2, \Lambda = 0.1$).

where we fixed $t_c \lll t_\Lambda$ in Regions I, II, and III, and $t_\Lambda \lll t_c$ in Regions IV and V. In the cases of Regions IV and V, we do not need to consider the size of t_c relative to t_{obs} , as curvature domination never occurs when $t_\Lambda \lll t_c$. We then plotted the calculable parts of the probability distribution, namely $t_\Lambda^{-2} M_{CP}$, for each region and a variety of (p, q, Q, Λ) to see if there were any discernible patterns in the results.

We found that the qualitative results are largely independent of the number of compact dimensions q (regardless of the total number of dimensions $D = p + 2 + q$), and the values of Q and Λ . The overall trends in the probability distribution are instead largely determined by the number $p + 1$ of large dimensions in the nucleated bubbles. These results are discussed in Sections VI A 1-VI A 3.

1. The case $p = 2$

As may be expected, in the case $p = 2$, which corresponds to a (3+1)-dimensional universe (with the possibility of q small dimensions compactified on a sphere), our results are similar to those of [22, 27]. Figures 3-7 show typical probability distributions in the case $p = 2$ for different values of the timescales t_{obs}, t_c, t_Λ . We see that in Region I, corresponding to $t_{obs} < t_c < t_\Lambda$, the probability remains almost constant over $\log t_\Lambda$, but increases with decreasing $\log t_c$. In Region II, corresponding to $t_c < t_{obs} < t_\Lambda$, the probability remains almost constant over $\log t_\Lambda$, but increases with increasing $\log t_c$. In Region III, corresponding to $t_c < t_\Lambda < t_{obs}$, the probability increases with both $\log t_\Lambda$ and $\log t_c$. In Region IV, corresponding to $t_\Lambda < t_{obs}$, the probability remains constant over $\log t_c$ but increases with $\log t_\Lambda$, whereas in Region V, corresponding to $t_{obs} < t_\Lambda$, the probability remains constant over $\log t_c$ and decreases as $\log t_\Lambda$ increases.

This information allows us to draw the force diagram for the probability distribution over $\log t_c$ and $\log t_\Lambda$ for fixed t_{obs} , where we have assumed that the factor $g(\log t_c) \times \alpha(\log t_{obs}, \log t_c, \log t_\Lambda)$ do *not* provide the leading contribution to the probability of observations. We see that for any fixed t_{obs} , the maximum of the probability distribution lies along the lines $\log t_{obs} \sim \log t_\Lambda$ and $\log t_{obs} \sim \log t_c$. By assuming that $g(\log t_c)$ decreases mildly, like an inverse power of $\log t_c$ [28], and by making mild assumptions on the form of α , as given in [22, 27], we can predict that the maximum

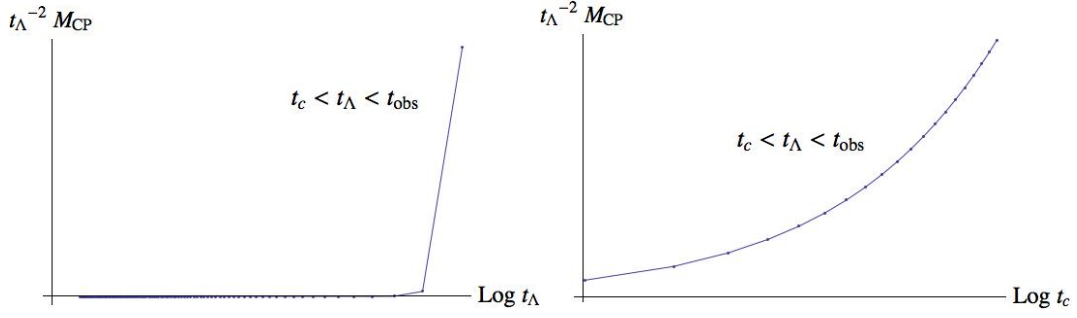


FIG. 5: Typical probability distributions obtained using the causal patch cutoff over $\log t_\Lambda$ for fixed $\log t_c$, and $\log t_c$ for fixed $\log t_\Lambda$, in the case $p = 2$, in Region III of parameter space, corresponding to $t_c < t_\Lambda < t_{obs}$. The specific parameters used here are ($p = 2, q = 2, Q = 3.2, \Lambda = 0.1$).

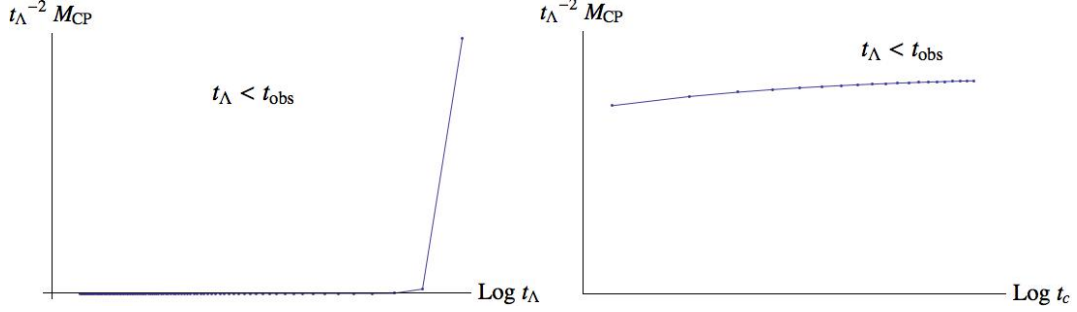


FIG. 6: Typical probability distributions obtained using the causal patch cutoff over $\log t_\Lambda$ for fixed $\log t_c$, and $\log t_c$ for fixed $\log t_\Lambda$, in the case $p = 2$, in Region IV of parameter space, corresponding to $t_\Lambda < t_{obs}$. The specific parameters used here are ($p = 2, q = 2, Q = 3.2, \Lambda = 0.1$).

of the probability distribution, when all three timescales are allowed to vary, is at

$$\log t_{obs} \sim \log t_c \sim \log t_\Lambda \sim \log t_\Lambda^{max}, \quad (35)$$

where $\log t_\Lambda^{max}$ corresponds to the smallest cosmological constant in the landscape, when considering bubbles with $p+1 = 3$ large dimensions. This scale is set by the number \mathcal{N} of such vacua in the landscape, according to $t_\Lambda^{max} \sim \mathcal{N}^{1/2}$.

2. The case $p \geq 3$

In the case $p \geq 3$, which corresponds to universes with a larger number of large dimensions than our own, we obtain slightly different results. Figures 9-13 show typical probability distributions in the case $p = 3$ for different values of

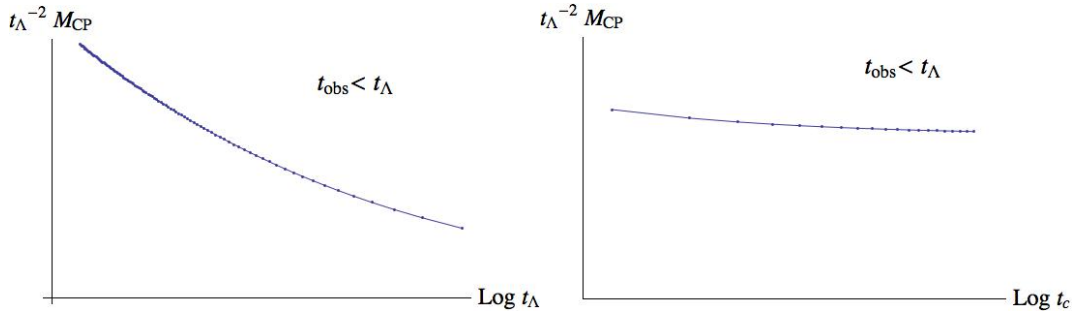


FIG. 7: Typical probability distributions obtained using the causal patch cutoff over $\log t_\Lambda$ for fixed $\log t_c$, and $\log t_c$ for fixed $\log t_\Lambda$, in the case $p = 2$, in Region V of parameter space, corresponding to $t_{obs} < t_\Lambda$. The specific parameters used here are ($p = 2, q = 2, Q = 3.2, \Lambda = 0.1$).

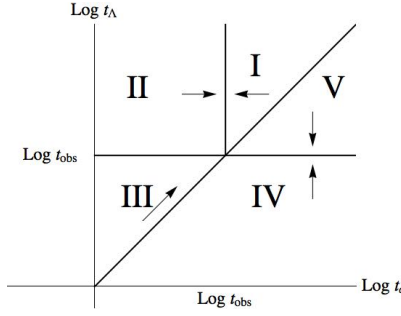


FIG. 8: The force diagram for the probability distribution when $p = 2$ for fixed t_{obs} , obtained using the causal patch measure. The arrows indicate directions of increasing probability. The distribution is peaked along the degenerate half-lines forming the boundary between Regions I and II.

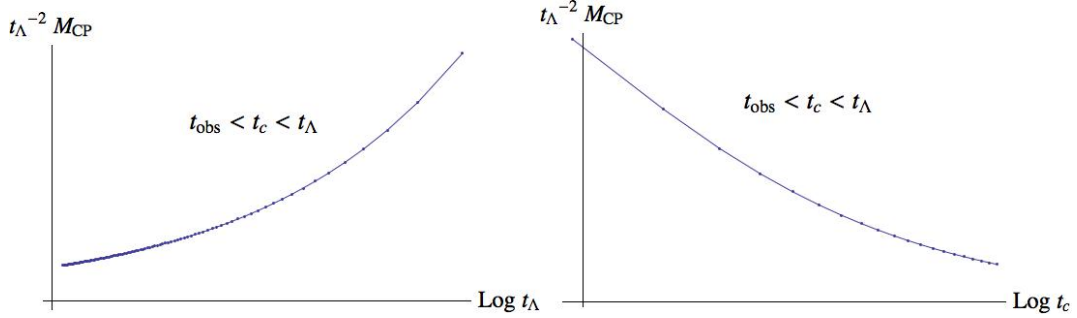


FIG. 9: Typical probability distributions obtained using the causal patch cutoff over $\log t_\Lambda$ for fixed $\log t_c$, and $\log t_c$ for fixed $\log t_\Lambda$, in the case $p = 3$, in Region I of parameter space, corresponding to $t_{obs} < t_c < t_\Lambda$. The specific parameters used here are ($p = 3, q = 2, Q = 3.2, \Lambda = 0.1$).

the timescales t_{obs}, t_c, t_Λ . We see that in Region I, corresponding to $t_{obs} < t_c < t_\Lambda$, the probability increases with $\log t_\Lambda$, but decreases with $\log t_c$. In Region II, corresponding to $t_c < t_{obs} < t_\Lambda$, the probability increases with both $\log t_\Lambda$ and $\log t_c$. In Region III, corresponding to $t_c < t_\Lambda < t_{obs}$, the probability is sharply peaked at large $\log t_\Lambda$ and increases with $\log t_c$. In Regions IV and V, corresponding to $t_\Lambda < t_{obs}$ and $t_{obs} < t_\Lambda$ respectively, the probability remains constant over $\log t_c$ but increases with $\log t_\Lambda$.

Once again, we can draw a force diagram for the probability distribution over $\log t_c$ and $\log t_\Lambda$ for fixed t_{obs} . We see that for any fixed t_{obs} , there is a runaway of the probability distribution towards large values of $\log t_\Lambda$, and the distribution is peaked along the line $\log t_{obs} \sim \log t_c$. Thus once again, as long as the factors $g(\log t_c) \times \alpha(\log t_{obs}, \log t_c, \log t_\Lambda)$ do not dominate the probability distribution, we can predict that the maximum probability,

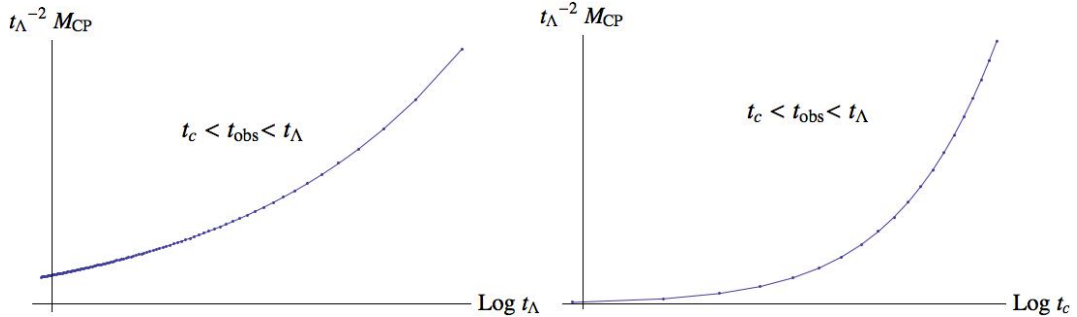


FIG. 10: Typical probability distributions obtained using the causal patch cutoff over $\log t_\Lambda$ for fixed $\log t_c$, and $\log t_c$ for fixed $\log t_\Lambda$, in the case $p = 3$, in Region II of parameter space, corresponding to $t_c < t_{obs} < t_\Lambda$. The specific parameters used here are ($p = 3, q = 2, Q = 3.2, \Lambda = 0.1$).

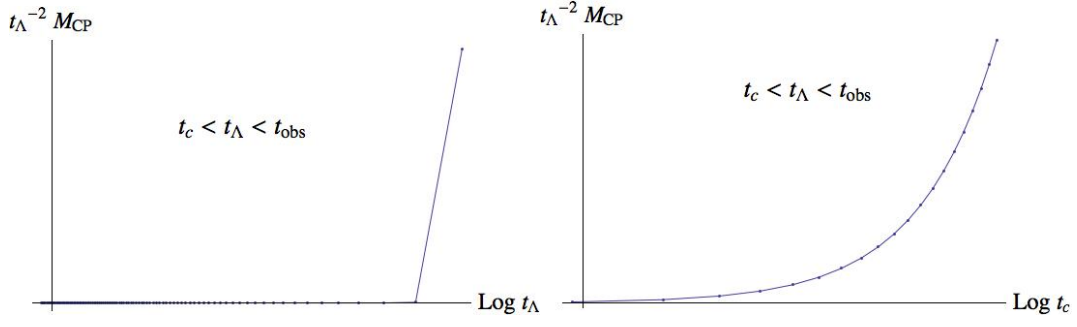


FIG. 11: Typical probability distributions obtained using the causal patch cutoff over $\log t_\Lambda$ for fixed $\log t_c$, and $\log t_c$ for fixed $\log t_\Lambda$, in the case $p = 3$, in Region III of parameter space, corresponding to $t_c < t_\Lambda < t_{obs}$. The specific parameters used here are ($p = 3, q = 2, Q = 3.2, \Lambda = 0.1$).

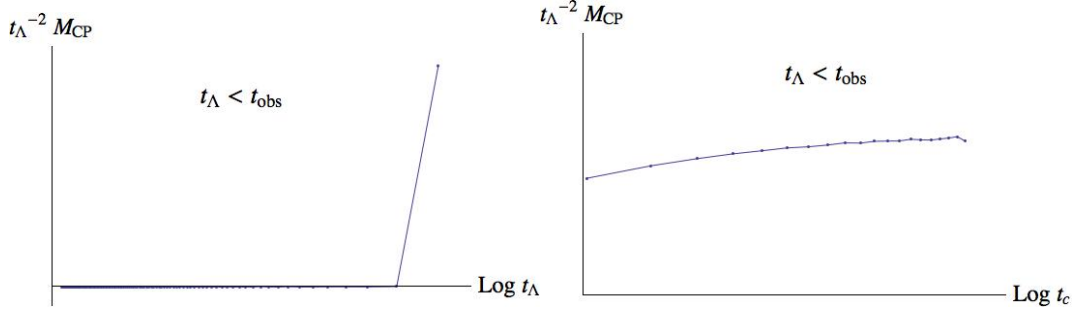


FIG. 12: Typical probability distributions obtained using the causal patch cutoff over $\log t_\Lambda$ for fixed $\log t_c$, and $\log t_c$ for fixed $\log t_\Lambda$, in the case $p = 3$, in Region IV of parameter space, corresponding to $t_\Lambda < t_{obs}$. The specific parameters used here are ($p = 3, q = 2, Q = 3.2, \Lambda = 0.1$).

when all three timescales are allowed to vary, is at

$$\log t_{obs} \sim \log t_c \sim \log t_\Lambda \sim \log t_\Lambda^{max}, \quad (36)$$

where $\log t_\Lambda^{max}$ corresponds to the smallest cosmological constant in the landscape, when considering bubbles with $p + 1$ large dimensions. So we see the same coincidence as in the case $p = 2$, even though the probability distribution itself looks different. As before, we see that the scale $\log t_{obs}$ is set by the smallest cosmological constant in the landscape, when considering bubbles with $p + 1 = 4$ large dimensions. This scale is set by the number \mathcal{N} of such vacua in the landscape, according to $t_\Lambda^{max} \sim \mathcal{N}^{1/2}$.

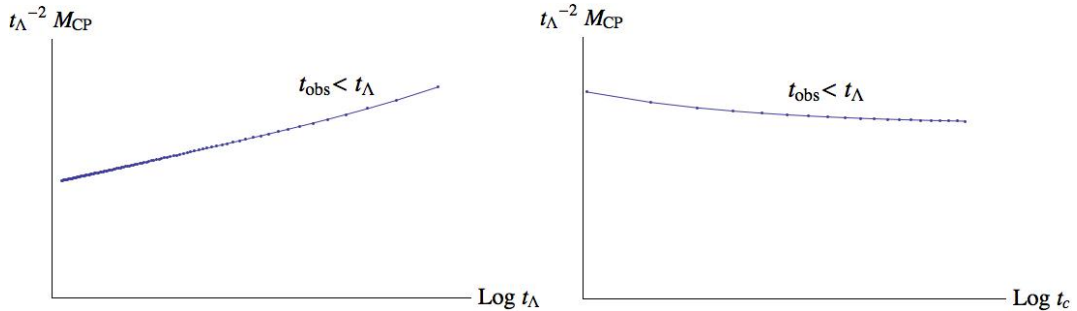


FIG. 13: Typical probability distributions obtained using the causal patch cutoff over $\log t_\Lambda$ for fixed $\log t_c$, and $\log t_c$ for fixed $\log t_\Lambda$, in the case $p = 3$, in Region V of parameter space, corresponding to $t_{obs} < t_\Lambda$. The specific parameters used here are ($p = 3, q = 2, Q = 3.2, \Lambda = 0.1$).

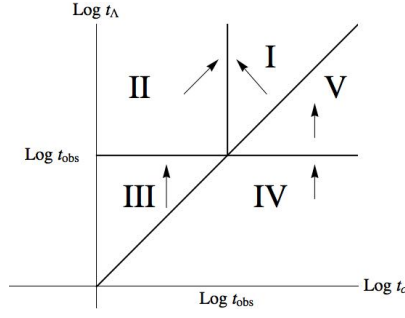


FIG. 14: The force diagram for the probability distribution when $p \geq 3$ for fixed t_{obs} , obtained using the causal patch measure. The arrows indicate directions of increasing probability. The distribution exhibits a runaway towards large t_Λ and $t_c \sim t_{obs}$.

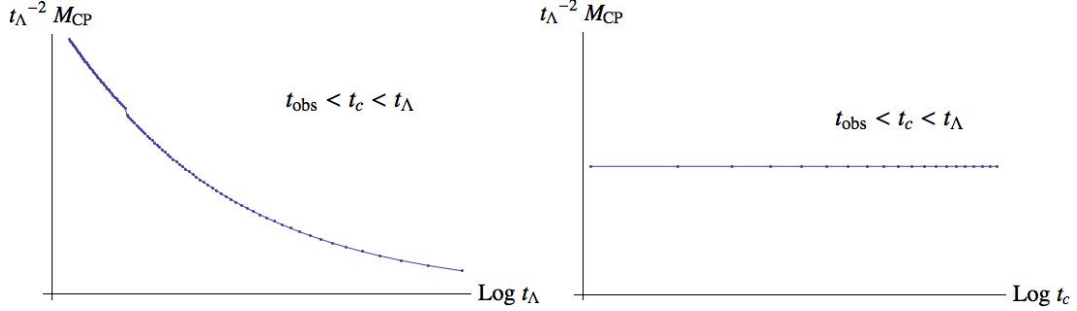


FIG. 15: Typical probability distributions obtained using the causal patch cutoff over $\log t_\Lambda$ for fixed $\log t_c$, and $\log t_c$ for fixed $\log t_\Lambda$, in the case $p = 1$, in Region I of parameter space, corresponding to $t_{obs} < t_c < t_\Lambda$. The specific parameters used here are ($p = 1, q = 3, Q = 40.1, \Lambda = 0.1$).

3. The case $p = 1$

Finally we consider the case $p = 1$, which covers universes with one fewer large dimension than our own. Figures 3-7 show typical probability distributions in the case $p = 1$ for different values of the timescales t_{obs}, t_c, t_Λ . We see that in Regions I and II, corresponding to $t_{obs} < t_c < t_\Lambda$ and $t_c < t_{obs} < t_\Lambda$ respectively, the probability decreases as $\log t_\Lambda$ increases, but remains constant over $\log t_c$. In Region III, corresponding to $t_c < t_\Lambda < t_{obs}$, the probability decreases with $\log t_\Lambda$, seeming to reach a local maximum near the minimum value of $\log t_\Lambda$, and remains constant over $\log t_c$. In Region IV, corresponding to $t_\Lambda < t_{obs}$, the probability remains constant over $\log t_c$ but decreases with $\log t_\Lambda$, whereas in Region V, corresponding to $t_{obs} < t_\Lambda$, the probability remains constant over $\log t_c$ and increases as $\log t_\Lambda$ increases.

We can now draw the force diagram for the probability distribution over $\log t_c$ and $\log t_\Lambda$ for fixed t_{obs} . We see that for any fixed t_{obs} , there is a runaway of the probability distribution towards small values of $\log t_\Lambda$ in Regions I,

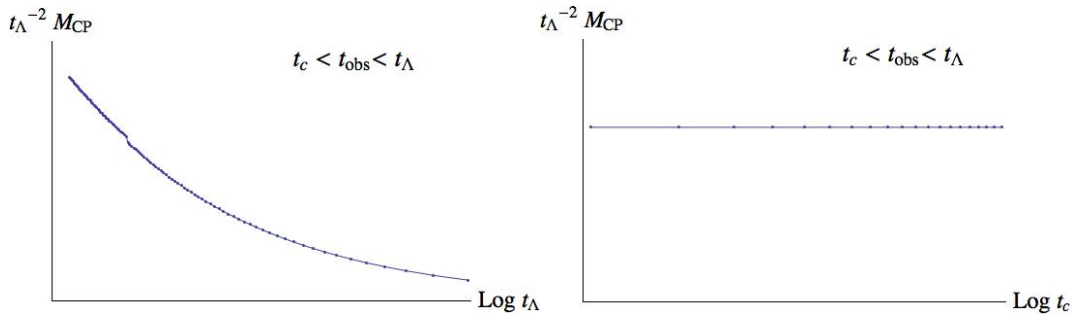


FIG. 16: Typical probability distributions obtained using the causal patch cutoff over $\log t_\Lambda$ for fixed $\log t_c$, and $\log t_c$ for fixed $\log t_\Lambda$, in the case $p = 1$, in Region II of parameter space, corresponding to $t_c < t_{obs} < t_\Lambda$. The specific parameters used here are ($p = 1, q = 3, Q = 40.1, \Lambda = 0.1$).

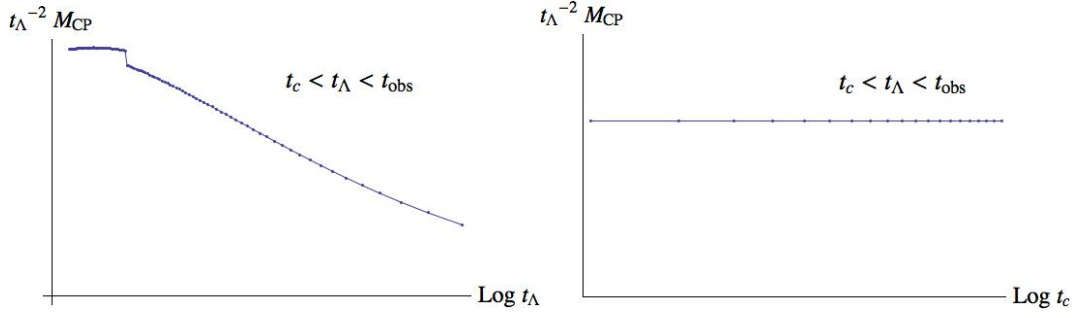


FIG. 17: Typical probability distributions obtained using the causal patch cutoff over $\log t_\Lambda$ for fixed $\log t_c$, and $\log t_c$ for fixed $\log t_\Lambda$, in the case $p = 1$, in Region III of parameter space, corresponding to $t_c < t_\Lambda < t_{obs}$. The specific parameters used here are ($p = 1, q = 3, Q = 40.1, \Lambda = 0.1$).

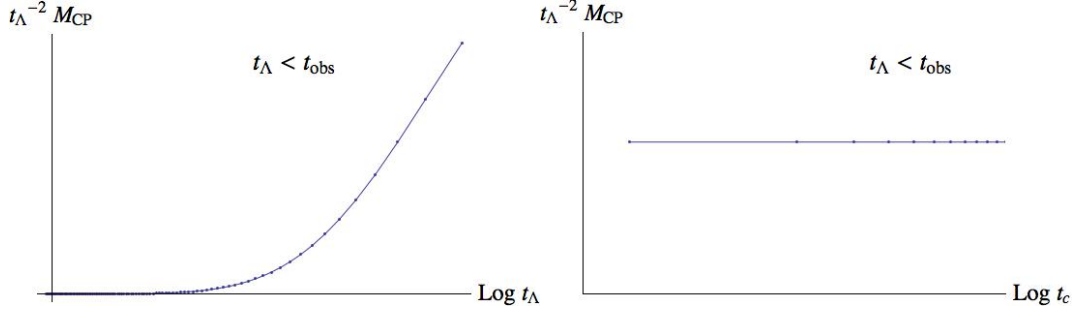


FIG. 18: Typical probability distributions obtained using the causal patch cutoff over $\log t_\Lambda$ for fixed $\log t_c$, and $\log t_c$ for fixed $\log t_\Lambda$, in the case $p = 1$, in Region IV of parameter space, corresponding to $t_\Lambda < t_{obs}$. The specific parameters used here are ($p = 1, q = 3, Q = 40.1, \Lambda = 0.1$).

II, and III, and the distribution is peaked along the line $\log t_{obs} \sim \log t_\Lambda$ in Regions IV and V. This situation is more complicated than in the cases $p \geq 2$, as we cannot make any definitive statements about coincidences of the timescales without more detailed calculations.

B. The fat geodesic measure

For the fat geodesic measure, we can use the fact that we count observations in a fixed physical volume around the geodesic, and the solution for $a(t)$ found using the Friedmann equation, to determine the volume available to observers living at t_{obs} . Since we are counting observers in a fixed physical volume, the mass of observers within the

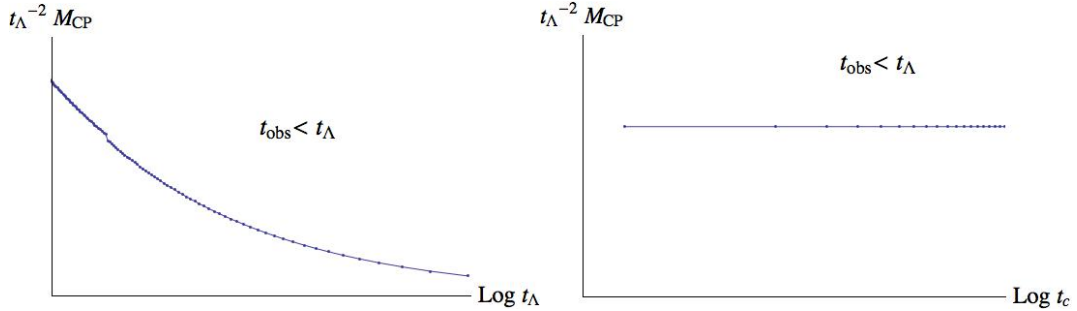


FIG. 19: Typical probability distributions obtained using the causal patch cutoff over $\log t_\Lambda$ for fixed $\log t_c$, and $\log t_c$ for fixed $\log t_\Lambda$, in the case $p = 1$, in Region V of parameter space, corresponding to $t_{obs} < t_\Lambda$. The specific parameters used here are ($p = 1, q = 3, Q = 40.1, \Lambda = 0.1$).

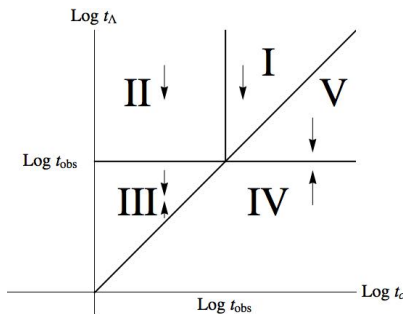


FIG. 20: The force diagram for the probability distribution obtain when $p = 1$ for fixed t_{obs} , obtained using the causal patch measure. The arrows indicate directions of increasing probability. The distribution is peaked along $\log t_{obs} \sim \log t_{\Lambda}$ in Regions IV and V, and exhibits a runaway towards small $\log t_{\Lambda}$ in the rest of parameter space.

cutoff region is proportional to the matter density:

$$M_{FG} \alpha \rho_m \sim \frac{t_c^{p-1}}{a^{p+1}}. \quad (37)$$

The probability distribution of observations made in the landscape is then given by (28), but with M_{FG} , the mass of observers inside the region defined by the fat geodesic cutoff, replacing M_{CP} , the mass of observers inside the region defined by the causal patch cutoff.

As with the causal patch cutoff, we scanned over a range of t_{Λ} by varying the parameters p , q , Q , and Λ , and solved the differential equations for $a(t)$ and $\phi(t)$ for a large range of t_{Λ} and t_c (where t_c was input by hand), and then calculated M_{FG} for a range of t_{obs} , choosing values for the three time scales so that they were well separated. We considered the same Regions I – V of parameter space as with the causal patch measure. We then plotted the calculable parts of the probability distribution, namely $t_{\Lambda}^{-2} M_{FG}$, for each region and a variety of (p, q, Q, Λ) to see if there were any discernible patterns in the results.

As with the causal patch measure, we found that the qualitative results depend only on the number $p + 1$ of large dimensions. However, unlike the causal patch measure, in the case of the fat geodesic measure the shape of the probability distribution is the same in all cases where the number $p + 1$ of large dimensions is ≥ 3 . These results are discussed in Sections VIB 1-VIB 2.

1. The case $p \geq 2$

In the case $p \geq 2$, our results are similar to those of [22, 27] in the case $p = 2$. Figures 21-25 show typical probability distributions in the case $p \geq 2$ for different values of the timescales $t_{obs}, t_c, t_{\Lambda}$. We see that in Region I, corresponding to $t_{obs} < t_c < t_{\Lambda}$, the probability remains constant over $\log t_c$, but decreases with $\log t_{\Lambda}$. In Region II, corresponding to $t_c < t_{obs} < t_{\Lambda}$, the probability decreases with $\log t_{\Lambda}$, but increases with $\log t_c$. In Region III, corresponding to $t_c < t_{\Lambda} < t_{obs}$, the probability increases with both $\log t_{\Lambda}$ and $\log t_c$. In Region IV, corresponding to $t_{\Lambda} < t_{obs}$, the probability remains constant over $\log t_c$ but increases with $\log t_{\Lambda}$, whereas in Region V, corresponding to $t_{obs} < t_{\Lambda}$, the probability remains constant over $\log t_c$ and decreases as $\log t_{\Lambda}$ increases.

This information allows us to draw the force diagram for the probability distribution over $\log t_c$ and $\log t_{\Lambda}$ for fixed t_{obs} , where we have assumed that the factor $g(\log t_c) \times \alpha(\log t_{obs}, \log t_c, \log t_{\Lambda})$ do *not* provide the leading contribution to the probability of observations. We see that for any fixed t_{obs} , the maximum of the probability distribution lies along the line separating Regions IV and V. A mild assumption on the prior probability distribution that favors small $\log t_c$ [22, 27] thus predicts the coincidence

$$\log t_{obs} \sim \log t_c \sim \log t_{\Lambda}. \quad (38)$$

We have confirmed numerically that M_{FG} decreases with t_{obs} . Assuming that the factor $g(\log t_{obs})$ in (28) also decreases with t_{obs} , and that $\alpha(\log t_{obs})$ does not grow too quickly with t_{obs} , we can say that there is a strong preference for t_{obs} , and thus t_{Λ} , to be small.

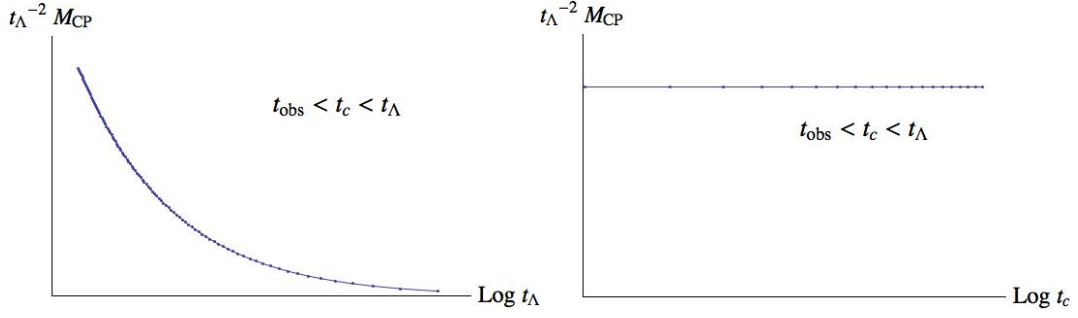


FIG. 21: Typical probability distributions obtained using the fat geodesic cutoff over $\log t_\Lambda$ for fixed $\log t_c$, and $\log t_c$ for fixed $\log t_\Lambda$, in the case $p \geq 2$, in Region I of parameter space, corresponding to $t_{obs} < t_c < t_\Lambda$. The specific parameters used here are ($p = 2, q = 2, Q = 3.2, \Lambda = 0.1$).

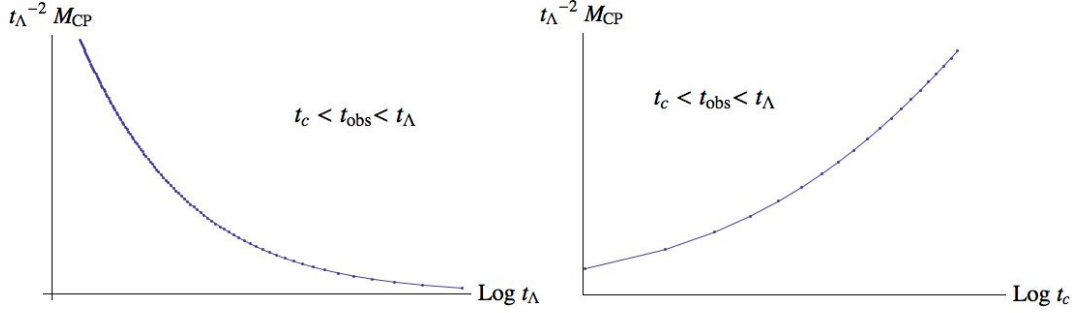


FIG. 22: Typical probability distributions obtained using the fat geodesic cutoff over $\log t_\Lambda$ for fixed $\log t_c$, and $\log t_c$ for fixed $\log t_\Lambda$, in the case $p \geq 2$, in Region II of parameter space, corresponding to $t_c < t_{obs} < t_\Lambda$. The specific parameters used here are ($p = 2, q = 2, Q = 3.2, \Lambda = 0.1$).

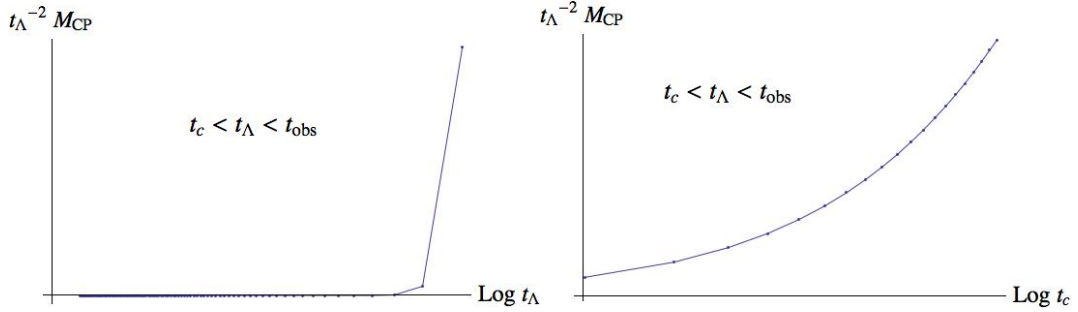


FIG. 23: Typical probability distributions obtained using the fat geodesic cutoff over $\log t_\Lambda$ for fixed $\log t_c$, and $\log t_c$ for fixed $\log t_\Lambda$, in the case $p \geq 2$, in Region III of parameter space, corresponding to $t_c < t_\Lambda < t_{obs}$. The specific parameters used here are ($p = 2, q = 2, Q = 3.2, \Lambda = 0.1$).

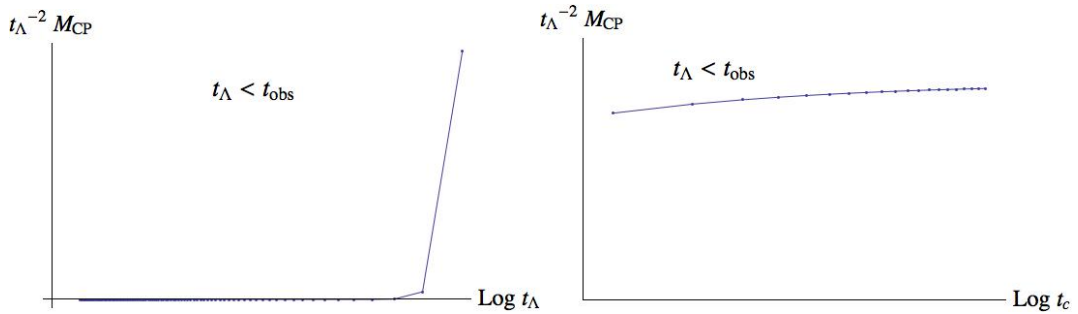


FIG. 24: Typical probability distributions obtained using the fat geodesic cutoff over $\log t_\Lambda$ for fixed $\log t_c$, and $\log t_c$ for fixed $\log t_\Lambda$, in the case $p \geq 2$, in Region IV of parameter space, corresponding to $t_\Lambda < t_{obs}$. The specific parameters used here are ($p = 2, q = 2, Q = 3.2, \Lambda = 0.1$).

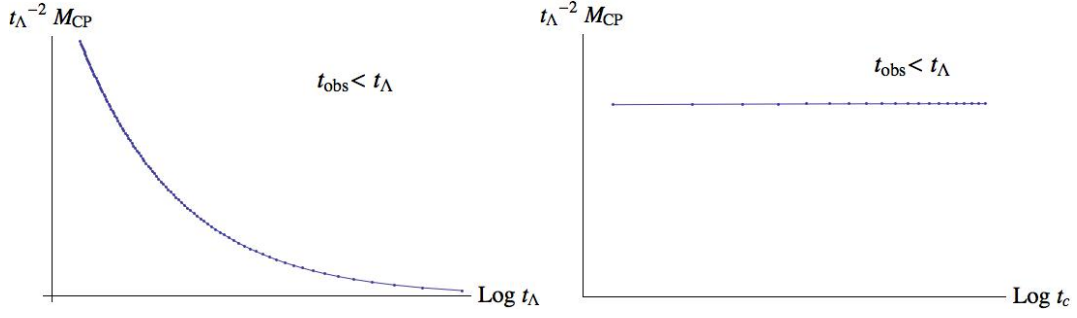


FIG. 25: Typical probability distributions obtained using the fat geodesic cutoff over $\log t_\Lambda$ for fixed $\log t_c$, and $\log t_c$ for fixed $\log t_\Lambda$, in the case $p \geq 2$, in Region V of parameter space, corresponding to $t_{obs} < t_\Lambda$. The specific parameters used here are ($p = 2, q = 2, Q = 3.2, \Lambda = 0.1$).

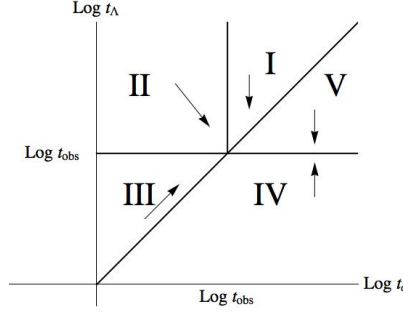


FIG. 26: The force diagram for the probability distribution when $p \geq 2$ for fixed t_{obs} , obtained using the fat geodesic cutoff. The arrows indicate directions of increasing probability. The distribution is peaked along the line separating Regions IV and V.

2. The case $p = 1$

Finally we consider the case $p = 1$, which covers universes with one fewer large dimension than our own. Figures 21-25 show typical probability distributions in the case $p = 1$ for different values of the timescales t_{obs}, t_c, t_Λ . We see that in all the Regions I – V, the probability distribution is constant over $\log t_c$. In Regions I – III and Region V, the probability decreases with $\log t_\Lambda$, whereas in Region IV the probability increases with $\log t_\Lambda$ to reach a local maximum at some large value of $\log t_\Lambda$ at the upper limit of its range, such that $t_\Lambda < t_{obs}$.

We can now draw the force diagram for the probability distribution over $\log t_c$ and $\log t_\Lambda$ for fixed t_{obs} . We see that for any fixed t_{obs} , there is a runaway of the probability distribution towards small values of $\log t_\Lambda$ in Regions I, II, III, and V. In Region IV, the probability distribution increases with increasing $\log t_\Lambda$ towards a local maximum near the top of the range of t_Λ , when $t_\Lambda < t_{obs}$ and $t_\Lambda \ll t_c$. This situation is more complicated than in the cases $p \geq 2$,

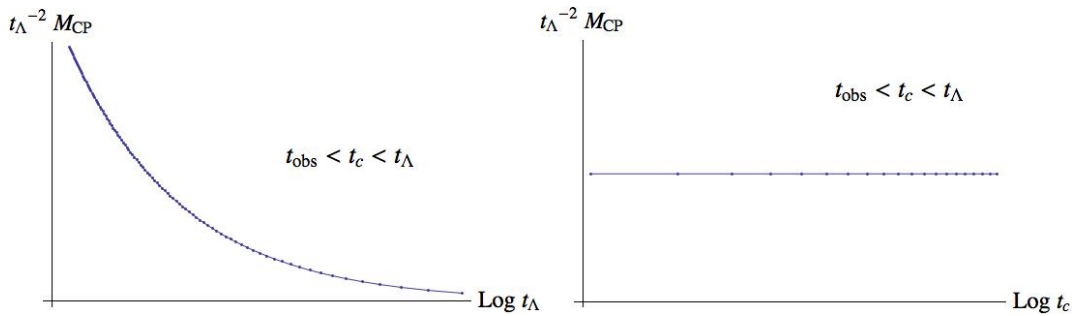


FIG. 27: Typical probability distributions obtained using the fat geodesic cutoff over $\log t_\Lambda$ for fixed $\log t_c$, and $\log t_c$ for fixed $\log t_\Lambda$, in the case $p = 1$, in Region I of parameter space, corresponding to $t_{obs} < t_c < t_\Lambda$. The specific parameters used here are ($p = 1, q = 3, Q = 40.1, \Lambda = 0.1$).

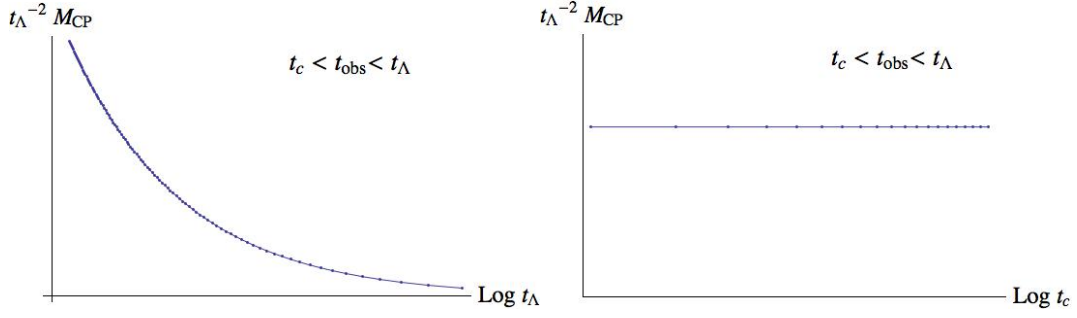


FIG. 28: Typical probability distributions obtained using the fat geodesic cutoff over $\log t_\Lambda$ for fixed $\log t_c$, and $\log t_c$ for fixed $\log t_\Lambda$, in the case $p = 1$, in Region II of parameter space, corresponding to $t_c < t_{obs} < t_\Lambda$. The specific parameters used here are ($p = 1, q = 3, Q = 40.1, \Lambda = 0.1$).

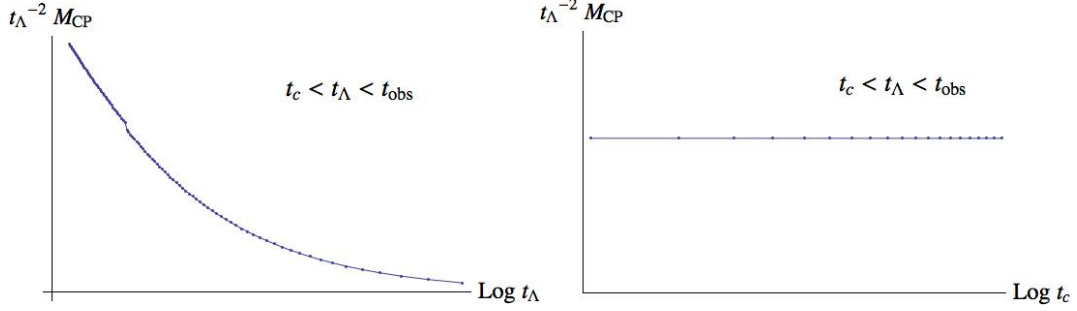


FIG. 29: Typical probability distributions obtained using the fat geodesic cutoff over $\log t_\Lambda$ for fixed $\log t_c$, and $\log t_c$ for fixed $\log t_\Lambda$, in the case $p = 1$, in Region III of parameter space, corresponding to $t_c < t_\Lambda < t_{obs}$. The specific parameters used here are ($p = 1, q = 3, Q = 40.1, \Lambda = 0.1$).

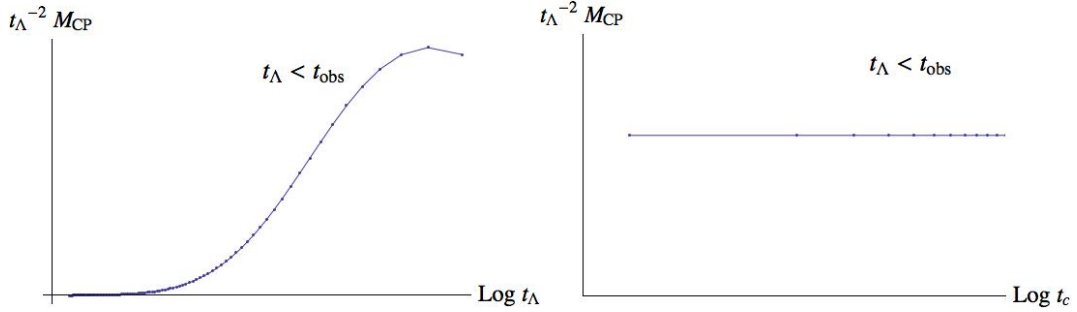


FIG. 30: Typical probability distributions obtained using the fat geodesic cutoff over $\log t_\Lambda$ for fixed $\log t_c$, and $\log t_c$ for fixed $\log t_\Lambda$, in the case $p = 1$, in Region IV of parameter space, corresponding to $t_\Lambda < t_{obs}$. The specific parameters used here are ($p = 1, q = 3, Q = 40.1, \Lambda = 0.1$).

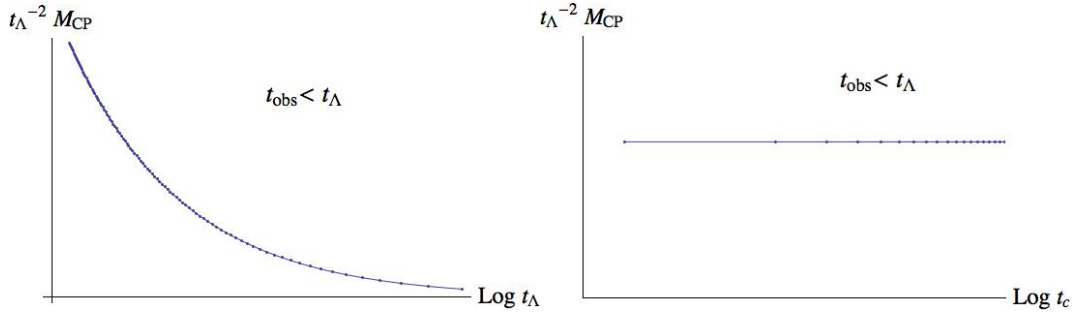


FIG. 31: Typical probability distributions obtained using the fat geodesic cutoff over $\log t_\Lambda$ for fixed $\log t_c$, and $\log t_c$ for fixed $\log t_\Lambda$, in the case $p = 1$, in Region V of parameter space, corresponding to $t_{obs} < t_\Lambda$. The specific parameters used here are ($p = 1, q = 3, Q = 40.1, \Lambda = 0.1$).

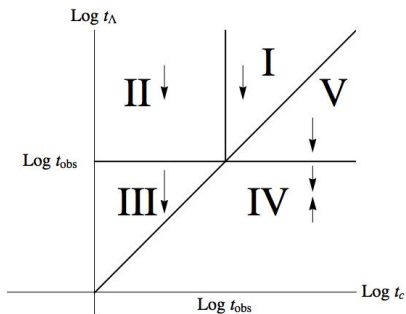


FIG. 32: The force diagram for the probability distribution obtained using the fat geodesic cutoff when $p = 1$ for fixed t_{obs} , obtained using the fat geodesic cutoff. The arrows indicate directions of increasing probability. The distribution is peaked along $\log t_{obs} \sim \log t_{\Lambda}$ in Regions IV and V, and exhibits a runaway towards small $\log t_{\Lambda}$ in the rest of parameter space.

as we cannot make any definitive statements about coincidences of the timescales without more detailed calculations and better knowledge of prior probabilities.

VII. CONCLUSION

In conclusion, we find that when the causal patch measure is generalized to a multi-dimensional multiverse, the coincidence of the timescales $t_{obs} \sim t_{\Lambda} \sim t_c$, and the relation of the smallness of the cosmological constant to the size of the landscape, appears to be something that is universal for the case of $p + 1$ -large dimensions when $p \geq 2$, and is not merely a consequence of the fact that we find ourselves in a vacuum with three large spatial dimensions. However, this coincidence occurs for a different reason in the case when $p = 2$ compared to when $p \geq 3$, as the probability distribution of observations has very different properties in the two cases. When the fat geodesic cutoff is generalized to a multi-dimensional multiverse, we find that the measure is even more robust: in addition to predicting the coincidence of the timescales $t_{obs} \sim t_{\Lambda} \sim t_c$ in all cases when the parameter $p \geq 2$, the shape of the probability distribution of observations is independent of the value of p . This makes intuitive sense when you consider that the generalization of the fat geodesic cutoff gives the same weighting to any unit of proper volume within a multiverse, regardless of the number of large dimensions. Thus, the probability distribution of observations remains independent of the number of large dimensions.

There are many possibilities for further investigations along these lines. For example, although we have argued that the multiverse model we have considered is fairly generic, it could be worthwhile to investigate other models of multiverses with multi-dimensional vacua to see if the same patterns emerge, to make sure that these results are not model-dependent. It would also be profitable to carry out a more detailed analysis of the probability distribution in this model, to see if more distinctive features of the distribution could be uncovered in addition to identifying the maxima. It would be interesting to see, for instance, whether the agreement between $\log t_{obs}$, $\log t_{\Lambda}$, and $\log t_c$ varies with p , or whether the distribution becomes more sharply peaked along the lines of coincidence as p varies. In general, the qualitative statement that the probability distribution of observations appears to change significantly when $p > 2$ compared to $p = 2$ suggests that it would be worthwhile to extend the study of measures from multiverses with only (3+1)-dimensional vacua to multiverses with vacua of many different dimensions.

VIII. ACKNOWLEDGMENTS

I would like to thank Professor Yasunori Nomura for helpful discussions on this subject and the measure problem in general, and for his comments on the draft of the manuscript. I would also like to thank Professor Lisa Randall for her guidance and suggestions in the early stages of this project.

-
- [1] A. H. Guth, Eternal inflation and its implications, *J. Phys. A* **A40**, 6811-6826 (2007), arXiv:hep-th/0702178.
 - [2] B. Freivogel, *Making predictions in the multiverse*, arXiv:1105.0244 [hep-th].
 - [3] R. Bousso, B. Freivogel, S. Leichenauer, V. Rosenhaus, *Boundary definition of a multiverse measure*, *Phys. Rev.* **D82**, 125032 (2010), arXiv:1005.2783 [hep-th].

- [4] S. R. Coleman, F. De Luccia, *Gravitational Effects on and of Vacuum Decay*, Phys. Rev. **D21**, 3305 (1980).
- [5] J. Garriga, D. Schwartz-Perlov, A. Vilenkin, S. Winitzki, *Probabilities in the inflationary multiverse*, JCAP 0601, 017 (2006), arXiv:hep-th/0509184 [hep-th].
- [6] A. De Simone, A. H. Guth, M. P. Salem, A. Vilenkin, *Predicting the cosmological constant with the scale-factor cutoff measure*, Phys. Rev. **D78**, 063520 (2008), arXiv:0805.2173 [hep-th].
- [7] R. Bousso, B. Freivogel, I-S. Yang, *Properties of the scale factor measure*, Phys. Rev. **D79**, 063513 (2009), arXiv:0808.3770 [hep-th].
- [8] B. Feldstein, L. J. Hall, T. Watari, *Density perturbations and the cosmological constant from inflationary landscapes*, Phys. Rev. **D72**, 123506 (2005), arXiv:hep-th/0506235.
- [9] J. Garriga, A. Vilenkin, *Anthropic prediction for Lambda and the Q catastrophe*, Prog. Theor. Phys. Suppl. 163, 245-257 (2006), hep-th/0508005.
- [10] M. L. Graesser, M. P. Salem, *The scale of gravity and the cosmological constant within a landscape*, Phys. Rev. **D76**, 043506 (2007), arXiv:astro-ph/0611694.
- [11] J. Garriga, A. Vilenkin, *Prediction and explanation in the multiverse*, Phys. Rev. **D77**, 043526 (2008), arXiv:0711.2559 [hep-th].
- [12] D. Schwartz-Perlov, A. Vilenkin, *Probabilities in the Bousso-Polchinski multiverse*, JCAP 0606, 010 (2006), arXiv:hep-th/0601162.
- [13] B. Freivogel, M. Kleban, M. Rodriguez Martinez and L. Susskind, *Observational consequences of a landscape*, JHEP 0603, 039 (2006), arXiv:hep-th/0505232.
- [14] R. Bousso, B. Freivogel, I-S. Yang, *Boltzmann babies in the proper time measure*, Phys. Rev. **D77**, 103514 (2008), arXiv:0712.3324 [hep-th].
- [15] A. Vilenkin, *Making predictions in an eternally inflating universe*, Phys. Rev. **D52**, 3365-3374 (1995), arXiv:gr-qc/9505031.
- [16] R. Bousso, B. Freivogel, I-S. Yang, *Eternal Inflation: The Inside Story*, Phys. Rev. **D74**, 103516 (2006), arXiv:hep-th/0606114.
- [17] R. Bousso, *Holographic probabilities in eternal inflation*, Phys. Rev. Lett. 97, 191302 (2006). arXiv:hep-th/0605263.
- [18] M. P. Salem, *Negative vacuum energy densities and the causal diamond measure*, Phys. Rev. **D80**, 023502 (2009), arXiv:0902.4485 [hep-th].
- [19] M. P. Salem, A. Vilenkin, *Phenomenology of the CAH+ Measure*, Phys. Rev. **D84**, 123520 (2011), arXiv:1107.4639 [hep-th].
- [20] S. Weinberg, *Anthropic bound on the cosmological constant*, Phys. Rev. Lett. **59** (1987) 2607.
- [21] S. B. Giddings, *The fate of four dimensions*, arXiv:hep-th/0303031
- [22] R. Bousso, B. Freivogel, S. Leichenauer, and V. Rosenhaus, *Geometric origin of coincidences and hierarchies in the landscape*, arXiv:1012.2869
- [23] D. Schwartz-Perlov and A. Vilenkin, *Measures for a Transdimensional Multiverse*, arXiv:1004.4567
- [24] Y. Nomura, *Physical Theories, Eternal Inflation, and Quantum Universe*, arXiv:1104.2324
- [25] Y. Nomuta, *Quantum Mechanics, Spacetime Locality, and Gravity*, arXiv:1110.4630
- [26] S. M. Carroll, M. C. Johnson, and L. Randall, *Dynamical compactification from de Sitter space*, arXiv:0904.3115.
- [27] R. Bousso, B. Freivogel, S. Leichenauer, and V. Rosenhaus, *A geometric solution of the coincidence problem, and the size of the landscape as the origin of hierarchy*, arXiv:1011.0714
- [28] S. Weinberg, *Anthropic bound on the cosmological constant*, Phys. Rev. Lett. 59 (1987) 2607.